Available online at www.sciencedirect.com
ScienceDirect
Catalysis Today 127 (2007) 278–290
CATALYSIS TODAY
www.elsevier.com/locate/cattod

# Pure hydrogen from pyrolysis oil using the steam-iron process

M.F. Bleeker *, S.R.A. Kersten, H.J. Veringa

*University of Twente, Department of Science and Technology, Enschede, The Netherlands*

Available online 15 June 2007

**Abstract**

The novelty of using pyrolysis oil in the steam-iron process to produce pure hydrogen is introduced. In this process, products of pyrolysis oil gasification are used to reduce iron oxides which are subsequently oxidized with steam, resulting in pure hydrogen. Two process alternatives are considered: (i) a once-through concept in which cheap iron oxide (in our case sintered pellets of natural iron ore, $Fe_2O_3$) is used in one cycle, before further processing in a blast furnace, and (ii) a continuous system, in which specially developed iron oxides (in our case an ammonia catalyst) are cycled between a reduction and oxidation reactor. By injecting pyrolysis oil in a fluidized bed filled with $Fe_3O_4$ at 800 °C, it has been shown that CO and $H_2$ as well as coke by the gasification reactions contribute to the reduction. Experiments including a complete redox cycle with the ammonia catalyst have shown that a hydrogen production in the oxidation of 0.84 N $m^3$/kg dry pyrolysis oil (LHV $H_2$/LHV oil = 0.4) can be obtained when the conversion of iron oxides are low (~1.0%). The gas produced in the reduction step under these conditions contains 38% of the heating value of the input and has an LHV of 7.8 MJ/N $m^3$ gas product. Deactivation of the iron oxides has been observed by a decreasing reduction rate in subsequent redox cycles. BET and SEM analysis showed a decrease in surface area, which could partly explain the observed deactivation.


*Keywords:* Pyrolysis oil; Steam-iron process; Hydrogen; Redox cycle

## 1. Introduction

The current worldwide hydrogen production approximates 50 million tonnes per year [1]. About 50% is used in the ammonia industry, 36% in oil refining and 8% in methanol production. Most of the hydrogen for these processes is produced on-site and only a small fraction, 6%, is consumed in chemical, food and metallurgical industries. Future demands for hydrogen are expected to increase, in existing industries and in new technologies like fuel cells. The increased refinery demand is driven by the need to produce cleaner transportation fuels in order to meet environmental regulations (e.g., low sulfur requirements) while the input slate continually shifts toward processing heavier crude [2]. Next to this, other growing sectors like fertilizers, biofuels and metallurgy will contribute to the increase in demand. There may be also a future demand of hydrogen as a transportation fuel in fuel cell driven vehicles. Using hydrogen as a transportation fuel results in an exhaust gas containing only water. Therefore, smog formation, especially in cities, now caused by the exhaust gases from fossil fuel combustion, will be prevented. An amount of 111 million tonnes of hydrogen needed for transportation only in the year 2050 in the USA is a prognosis that shows a possible immense growth [1]. To cover the projected hydrogen demand it is necessary to improve the hydrogen recovery in refineries and, eventually, to utilize other potential sources [3]. At this moment hydrogen is predominantly (48%) produced by the steam reforming of methane [4]. The price of this methane-based hydrogen depends for 70% or more on the price of the feedstock. In response to the increasing demand of hydrogen and the problems that go along with the use of fossil fuels, renewable alternatives, like biomass feedstocks, are being considered. Agricultural and forestry wastes are estimated to be energy equivalent to half of the current world's oil production [5]. This indicates that the potential of biomass as a $CO_2$ neutral feedstock for chemicals, fuels and hydrogen production is considerable. Hydrogen produced out of biomass can be used for all current applications including fuel cells. It is however also necessary to produce bio-based hydrogen to enable other biomass-to-fuel production routes. Diesel fuels, for example, can be produced by the Fischer–Tropsch process [6] from bio-based synthesis gas. However, the ratio of $H_2$/CO obtained by biomass gasification is typically between 0.8 and 1.6 while a $H_2$/CO ratio of at least 2 is required for Fischer–Tropsch

* Corresponding author. Tel.: +31 53 4894418; fax: +31 53 4894738.
*E-mail address:* m.f.bleeker@utwente.nl (M.F. Bleeker).

0920-5861/$ – see front matter 
doi:10.1016/j.cattod.2007.04.011

**Nomenclature**

| | |
|---|---|
| $d_p$ | particle diameter (μm) |
| $f$ | weight fraction |
| $\Delta G_r^0$ | reaction Gibbs energy (kJ/mol) |
| $\Delta H_r^0$ | reaction enthalpy (kJ/mol) |
| $L_{bed}$ | bed height (m) |
| $M$ | molecular weight (g/mol) |
| $M_{bed}$ | mass of the bed material (kg) |
| $P$ | pressure (Pa) |
| P-O | pyrolysis oil |
| $R$ | mass ratio of iron oxide and pyrolysis oil |
| $R_{gas}$ | gas constant (J/mol K) |
| $R_{ox}$ | mass ratio of iron oxide and steam |
| $S_0$ | amount of oxygen in iron oxide (mol) |
| $T$ | temperature (K) |
| $u_{mf}$ | minimum fluidization velocity (m/s) |
| $u_{reactor}$ | gas velocity in the fluidized bed reactor (m/s) |
| $V_{bed}$ | volume of the bed material ($m^3$) |
| $X$ | mole fraction |

*Greek letters*

| | |
|---|---|
| $\alpha(Fe_3O_4–Fe)$ | reduction degree of iron oxides |
| $\eta$ | energy efficiency calculated from the gas produced during reduction or oxidation and the oil injected (LHV MJ gas product/LHV MJ oil) |
| $\rho$ | density ($kg/m_3$) |
| $\tau$(bed) | residence time in the fluidized bed ($V_{bed} \times \varepsilon_{mf}/(\Phi_{v,in} + \Phi_{v,out})/2$) (s) |
| $\zeta_{C\ total}$ | conversion of carbon from the oil to the gas phase and deposited on the bed material |
| $\zeta_{C\ to\ gas}$ | conversion of carbon from the oil to the gas phase |
| $\zeta_{H_2O}$ | conversion of steam during oxidation |
| $\zeta_{H_2O,max}$ | highest conversion of steam during oxidation |
| $\zeta_{H_2O\ reacted\ with\ C}$ | conversion of steam by the reaction of steam with carbon |
| $\Phi$ | mol flow (mol/s) |
| $\Phi_m$ | mass flow (kg/s) |
| $\Phi_v$ | volumetric flow (N l/s) |

*Subscripts*

| | |
|---|---|
| C | oxygen |
| O | carbon |

synthesis [7]. Another example is the co-feeding/co-processing of liquefied biomass in a crude oil refinery. In this route hydrogen is required for deoxygenation and to increase the H/C ratio of bio-liquids [8].

Production processes for hydrogen out of biomass can be divided into biological/bio-chemical and thermo-chemical processes, with or without catalysis. The thermo-chemical processes are based on gasification and liquefaction. Thermal efficiencies for hydrogen production via gasification are estimated to range from 50 to 60% on HHV basis [9,10]. Purification of the gas from CO and $CO_2$ is needed and will be expensive. Therefore, alternative processes which require none or less purification can be beneficial. In this paper, a process is introduced in which pyrolysis oil is used in a redox cycle to produce pure hydrogen.

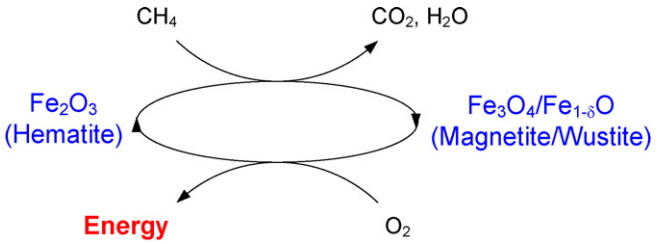


Fig. 1. Chemical looping combustion (CLC) with methane.

Pyrolysis oil might be an interesting intermediate energy carrier for the production of hydrogen from biomass. Pyrolysis oil can be produced with a yield of 65–75 wt.% out of solid biomass by the fast pyrolysis process. The pyrolysis liquid is usually dark brown and free flowing with a distinctive smoky smell. Chemically, it approximates to biomass in elemental composition and is composed of a very complex mixture of oxygenated hydrocarbons with an appreciable proportion of water (15–35 wt.%) [11,12]. Pyrolysis oil contains much less metals and minerals than raw biomass, which is beneficial for its catalytic upgrading. Other advantages of pyrolysis oil compared with solid biomass are its higher volumetric energy density (typically 20 $GJ/m^3$ versus 4 $GJ/m^3$) and the fact that liquids are generally easier to process.

The principle of using a redox cycle for the production of hydrogen was first used in the steam-iron process at the beginning of the 20th Century. The first manufacturers using the steam-iron process were Messerschmitt and Lane [13]. In those days, gas produced by the gasification of cokes was used to reduce iron oxides that were subsequently oxidized with steam for the production of pure hydrogen. At present the steam-iron process is not in use anymore for the production of hydrogen, because other processes are more economically efficient. However, some research activities are ongoing on the use of ‘‘cheap’’ hydro carbonaceous feedstocks as reducing agents, improved reactor concept and metal oxide used [14–19]. A recent example of a redox process is the development of chemical looping combustion (CLC) [20] (Fig. 1). In this process a redox cycle is applied to generate heat by oxidizing a reduced (by, e.g., methane) metal or metal oxide with air or oxygen. The benefit of this process is that a concentrated $CO_2$ stream, ready for sequestration, emerges without the need for air separation.

## 2. Steam-iron process with pyrolysis oil

For the production of hydrogen from pyrolysis oil two processes are considered: Concept 1: a looping process that recycles a certain amount of iron oxides (per unit of feed) between a reduction and oxidation reactor (Fig. 2A). Concept 2 is a once-through process that uses a batch of iron oxide for one reduction and oxidation step (Fig. 2B). In both processes, the gas produced in the reduction step can be used for heating

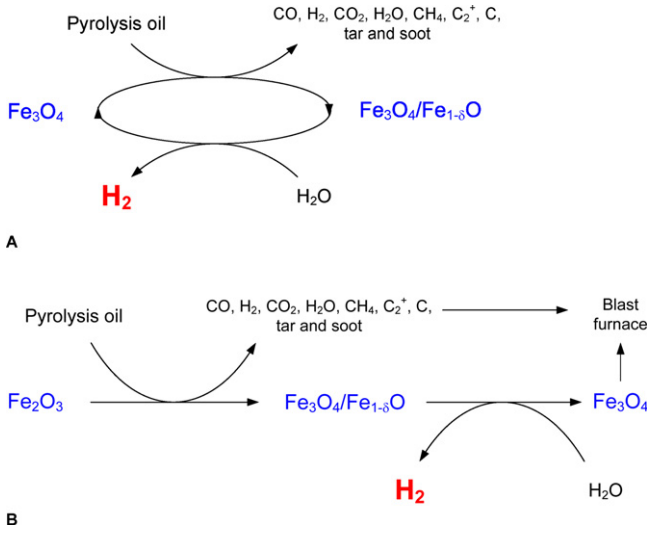


Fig. 2. Steam-iron process with pyrolysis oil: (A) recycling of iron oxide and (B) once-through process.

purposes (e.g., blast furnace) or can be upgraded to, for example, synthesis gas. The once-through concept may benefit from the possible heat integration near steel industries. It also reduces the burden on the lifetime of the iron oxide. Temperatures used for the steam-iron process are in general around 800 °C.

The reactants that are expected to contribute in the reduction of the iron oxides are CO, $H_2$ and solid carbon [21,22]. Reduction of iron oxides with hydrocarbons can take place, especially $Fe_2O_3$, but is slow for $Fe_3O_4$ and lower oxides [23]. Other products that are formed when pyrolysis oil is gasified, like $CH_4$ and $C_2^+$ will therefore only substantially contribute to the reduction of $Fe_3O_4$ if they are converted to CO and $H_2$ by, e.g., steam reforming reactions [18]. Normally pyrolysis oil contains 15–35 wt.% of $H_2O$, which would therefore be beneficial if the iron oxide works as a catalyst for steam reforming reactions of hydrocarbons and tars.

### 2.1. Reactions

The fresh iron oxide used consists of hematite ($Fe_2O_3$) and is initially reduced to $Fe_3O_4$ resulting mainly in $CO_2$, $H_2O$ and some $CH_4$. This was observed from experiments performed in the fluidized bed with pyrolysis oil or ethanol as reducing agent.

Table 1
Reactions with thermodynamic data at 827 °C

| | Reaction | $\Delta H^0_{r(T=827\,^\circ C)}$ (kJ/mol) | $\Delta G^0_{r(T=827\,^\circ C)}$ (kJ/mol) |
|---|---|---|---|
| 1 | $1.2Fe_3O_4 + CO \leftrightarrow 3.8Fe_{0.945}O + CO_2$ | 27 | −5.1 |
| 2 | $1.2Fe_3O_4 + H_2 \leftrightarrow 3.8Fe_{0.945}O + H_2O$ | 61 | −5.2 |
| 3 | $1.2Fe_3O_4 + C \leftrightarrow 3.8Fe_{0.945}O + CO$ | 197 | −27 |
| 4 | $Fe_{0.945}O + H_2 \leftrightarrow 0.945Fe + H_2O$ | 16 | 6.0 |
| 5 | $Fe_{0.945}O + CO \leftrightarrow 0.945Fe + CO_2$ | −18 | 5.9 |
| 6 | $Fe_{0.945}O + C \leftrightarrow 0.945Fe + CO$ | 152 | −16 |
| 7 | $C + 2H_2O \rightarrow CO_2 + 2H_2$ | 102 | −22 |
| 8 | $C + H_2O \rightarrow CO + H_2$ | 136 | −22 |

Oxidation of $Fe_3O_4/Fe_{1-\delta}O$ with steam to $Fe_2O_3$ is thermodynamically impossible ($\Delta G^0_r$ for the oxidation of $Fe_3O_4$ to $Fe_2O_3$ with steam is 58 kJ/mol $H_2O$ at $T = 327$ °C and 108 kJ/mol $H_2O$ at $T = 927$ °C); this can only be achieved when oxidation is performed with oxygen. Consequently, pyrolysis oil used for the reduction of $Fe_2O_3$ to $Fe_3O_4$ does not contribute to the production of hydrogen in the oxidation step.

As an example the reduction reaction of magnetite to wustite is given with the expected reducing compounds from pyrolysis oil gasification, CO, $H_2$ and C (Table 1). Wustite is iron deficient and the iron:oxygen ratio in wustite can range between 0.83 and 0.95 [24]. The thermodynamic data used in our calculations assumes that wustite is present as $Fe_{0.945}O$ [25]. The atomic composition of the iron oxides produced in the experiments was not measured. Further on in the text wustite will be denoted as $Fe_{0.945}O$ when used in thermodynamic calculations and as $Fe_{1-\delta}O$ in all other situations.

The reduction reactions of magnetite to wustite and especially the reduction with carbon are endothermic. The reduction of wustite with $H_2$ to metal iron is also endothermic except for the reduction of wustite to metal iron with CO.

Equilibrium calculations were performed for each of the reduction reactions that can take place individually (see Table 1). Thermodynamic data were taken from NIST/JANAF [25]. According to thermodynamics carbon reduces magnetite into wustite at temperatures >700 °C ($\Delta G$ reaction <0). The formed CO in this reaction (reaction (3), Table 1) can react further and contribute to the reduction via reaction (1).

The equilibrium constants for the reactions between the iron oxides and $H_2$–$H_2O$ or CO–$CO_2$ determines the ratio between $H_2/H_2O$ and $CO/CO_2$ at equilibrium, and thus the maximum CO and $H_2$ conversion in the reduction step and the maximum $H_2O$ conversion in the oxidation step. In Fig. 3 it can be seen that $Fe_{0.945}O$ is stable above temperatures of 573 °C. At lower temperatures it is thermodynamically favored to convert magnetite directly into metal iron. For example an $H_2/H_2O$ gas mixture with 50 vol.% $H_2$ at 800 °C has a reducing capacity to convert magnetite into wustite, but cannot reduce wustite to metal iron. The conversion of magnetite takes place at 800 °C

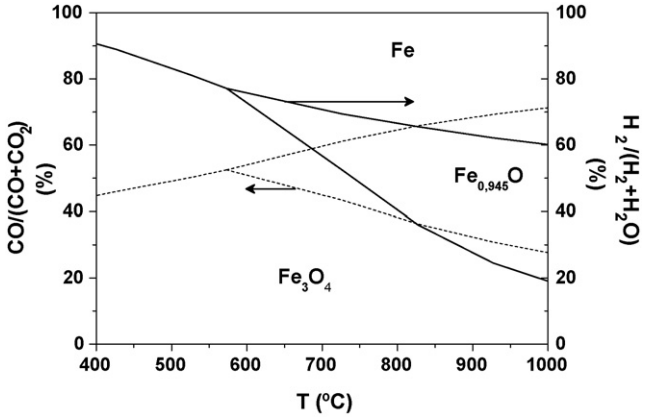


Fig. 3. Bauer–Glaessner diagram: equilibrium compositions of the gases involved in the redox reactions of $H_2/H_2O$ and $CO/CO_2$ with $F_3O_4$ (magnetite), $Fe_{0.945}O$ (wustite) and Fe.

with this mixture, until the gas phase reaches 40 vol.% $H_2$. The Bauer–Glaessner diagram [3] clearly shows that the total hydrogen production in the oxidation step is limited by the chemical equilibrium in the reduction step, because not all CO and $H_2$ produced from gasified pyrolysis oil can be used for reduction. Furthermore it shows that a higher equilibrium conversion of steam to hydrogen is expected during oxidation when metal iron is formed during reduction and at lower temperatures, which is beneficial for the efficiency of the process. The reaction rate, on the other hand, will be slower at lower temperatures.

## 3. Experimental

### 3.1. Set-up

The experimental set-up is shown in Fig. 4. The set-up consisted of a fluidized bed reactor (i.d. 0.078 m, $L$ 1 m). Hot fluidization gasses (nitrogen or air) and steam were entering the reactor in the lower conically shaped part of the reactor by four entrances. The preheated (reactor temperature) gasses and steam were blown tangentially along the wall of the reactor to enhance mixing of the gasses in the lower part of the reactor. Temperature sensors and differential pressure indicators were located along the wall of the reactor. Additional temperature sensors were measuring the temperature in the centre of the fluidized bed. Pyrolysis oil was fed with a dual head hose pump to the reactor via a cooled atomizer, which sprayed a cold nitrogen/pyrolysis oil mixture into the lower conical mixing zone of the reactor. The atomizer transformed the pyrolysis oil into a mist of small droplets via a spraying nozzle. The nozzle mixed the nitrogen and pyrolysis oil in an internal mixing chamber before entering the reactor. The atomizer was designed for a minimum water flow of 0.5 kg/h at ambient conditions. Cooling of the atomizer was necessary to prevent the pyrolysis oil from polymerizing, which may already occur at 200 °C, before entering the reactor. Therefore, the atomizer temperature was maintained below 100 °C, to prevent boiling of the water in the pyrolysis oil as well. The temperature of the atomizer head was measured with a temperature sensor.

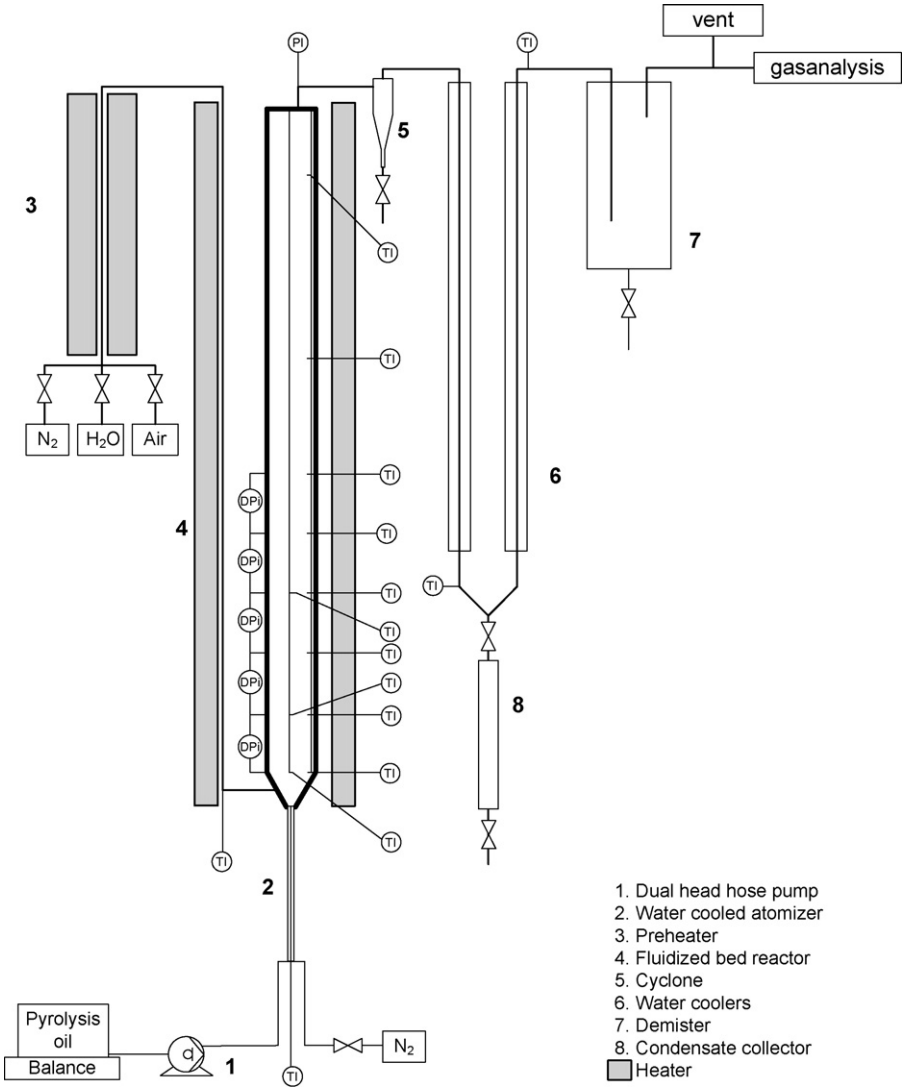


Fig. 4. Schematic overview of the fluidized bed set-up.

Table 2
Elemental composition and water content of the pyrolysis oil used

| Component | wt.% (wet) |
|---|---|
| C | 40.7 |
| H | 8.22 |
| O[a] | 50.9 |
| N | 0.14 |
| $H_2O$ | 28.28 |

[a] Determined by difference.

Gasses from the reactor passed through a small cyclone, to separate small particles that were entrained with the product gas. The amount of particles collected in the cyclone was measured after each reaction. Two water coolers condensed the water and other organic liquids that were formed during reaction. The amount of condensate was collected and weighed after the reaction. A demister was installed in case not all vapors were condensed in the coolers. Eventually a gas sample was pumped through the gas analysis unit. This unit included filters, to capture aerosols and other unwanted by products, a gas cooler operating at 5 °C, to maintain a constant analysis temperature through al experiments, and analyzers. Gasses were analyzed by online analyzers for CO, $CO_2$, $CH_4$ (IR) and $H_2$ (TCD). A gas chromatograph was used to analyze hydrocarbons ($C_2$ and $C_3$).

### 3.2. Materials

Pyrolysis oil from the pyrolysis of pine wood was obtained from the Biomass Technology Group (Enschede, the Netherlands). The composition of the used pyrolysis oil is given in Table 2.

Sand with an average particle size of 300 μm and density of 2400 kg/m$^3$ was used as bed material when non-catalytic pyrolysis oil gasification was studied.

Two types of iron oxides were used: (i) a catalytic iron oxide, normally used in the ammonia industry, obtained from the Boreskov Institute of Catalysis (Novosibirsk, Russia), and (ii) grinded sintered pellets, used for steel production in blast furnaces from CORUS (Ymuiden, The Netherlands). The compositions are given in Table 3.

### 3.3. Experimental procedures

#### 3.3.1. Pyrolysis oil gasification in a fluidized sand bed

The pyrolysis oil was sprayed at a constant flow rate in the fluidized bed reactor filled with sand particles. Additional hot nitrogen was used for fluidization. After injection of the pyrolysis oil, burning of the cokes on the sand particles was performed with air. The settings used for the gasification experiments are given in Table 4.

Table 3
Composition and properties of the iron oxides used

| | BIC (wt.%) | BF sintered pellets (wt.%) |
|---|---|---|
| $Fe_2O_3$ | 87.9 | 95.1 |
| $Cr_2O_3$ | 9.2 | |
| CuO | 2.7 | |
| $SiO_2$ | | 2.21 |
| MgO | | 1.47 |
| BET (m$^2$/g) | 31.2 | 0.19 |
| Average $d_p$ (mm) | 1.0 and 0.7 | 0.2 |

Table 4
Experimental settings for the gasification experiments in the fluidized sand bed

| | Gasification | Burning deposited coke |
|---|---|---|
| $\Phi_m$ pyrolysis oil (kg/h) | 0.5 | – |
| $\Phi_v$ $N_2$_atomizer (N l/min) | 6.1 | 6.1 |
| $\Phi_v$ $N_2$_hot (N l/min) | 6.0 | – |
| $\Phi_v$ air_hot (N l/min) | – | 3.9 |
| $u_{reactor}$ ($T$ = 800 °C)[a] (m/s) | 0.22 (9.7 × $u_{mf}$) | 0.14 (8 × $u_{mf}$) |
| $M_{bed}$ (kg) | 1.5 | 1.5 |
| $L_{bed}$ (m) | 0.21 | |

[a] Minimum fluidization velocity ($u_{mf}$) is calculated at 800 °C from [38].

The temperature in the reactor was influenced by pyrolysis oil injection and by endo- and exothermic reactions. Therefore, when an experiment was started the temperature in the reactor dropped or increased depending on the experiment performed. The temperature was measured at several places in the bed, to check temperature differences in the fluidized bed. Thermocouples in the centre (3) and near the wall of the reactor (4) showed never a higher $\Delta T$ than 5 °C during reaction (in sand and iron oxide bed). During the gasification of pyrolysis oil over a sand bed a time invariant temperature was obtained after several minutes. This temperature was defined as the reaction temperature.

#### 3.3.2. Redox cycle

One redox cycle consisted of a reduction and an oxidation step. In the first part of the reduction step pyrolysis oil was injected in the fluidized bed and additional hot nitrogen was injected for fluidization of the bed. In this step, pyrolysis oil was gasified and iron oxides were reduced (reduction I). In the second part of the reduction (reduction II), only hot nitrogen was introduced in the reactor to allow the slower reaction of deposited carbon and iron oxide to complete. The oxidation step was performed with hot steam and nitrogen injected at reactor temperature. When the hydrogen production was approaching zero (below 0.07 N l/min) steam injection was stopped and the redox cycle was finished. Settings used for the redox experiments are given in Table 5.

If iron oxide is used as bed material, an initial strong decrease in temperature was observed (max. 50 °C) in the reduction step (see Fig. 7), due to the endothermic reduction

Table 5
Experimental settings for the redox experiments with fluidized iron oxides

| | Reduction (I) | Reduction (II) | Oxidation |
|---|---|---|---|
| $\Phi_m$ pyrolysis oil (kg/h) | 0.5 | – | – |
| $\Phi_v$ $N_2$_atomizer (N l/min) | 6.1 | 6.1 | 2.2 |
| $\Phi_v$ $N_2$_hot (N l/min) | 5.0 | 5.0 | 2.0 |
| $\Phi_v$ $H_2O$_hot (kg/h) | – | – | 0.2 |
| $u_{reactor}$ ($T$ = 800 °C) (m/s) | 0.21 | 0.15 | 0.11 |
| $M_{bed}$ ($Fe_3O_4$; kg) | 1.7 | 1.7 | 1.7 |

reactions. During the second part of the reduction (no oil injection) the temperature rose again approaching the set-point of the controllers. The lowest temperature obtained in the bed during injection was defined as reactor temperature. When the oxidation was started a quick temperature increase towards a constant value (reaction temperature) was observed.

### 3.4. Atom balances, product yields and conversions

Mass balances were obtained from the measured gas composition, flow rate of the gaseous products and the amount of pyrolysis oil fed to the system. The gasses that were measured with the gas chromatograph and online analyzers used for the calculations were: $H_2$, $CH_4$, CO, $CO_2$, $C_2H_4$, $C_2H_6$, $C_3H_6$ and $C_3H_8$.

#### 3.4.1. Reduction and pyrolysis oil gasification

Two integral carbon balances are calculated. The carbon conversion, $\zeta_{\text{C to gas}}$, is defined as the amount of carbon transferred from the pyrolysis oil to gaseous products in reduction step I and in gasification tests in the fluidized sand bed. $\zeta_{\text{C to gas}}$ is calculated from the gasses formed during the pyrolysis oil injection period.

$$\zeta_{\text{C to gas}} = \frac{\int_{t_{\text{start oil injection}}+\tau_d}^{t_{\text{end oil injection}}+\tau_d} \left(\Phi_{CO}(t) + \Phi_{CO_2}(t) + \Phi_{CH_4}(t) + 2\Phi_{C_2H_4}(t) + 2\Phi_{C_2H_6}(t) + 3\Phi_{C_3H_6}(t) + 3\Phi_{C_3H_8}(t)\right) dt}{\int_{t_{\text{start oil injection}}}^{t_{\text{end oil injection}}} \left(\Phi_{\text{m,oil}}(t)\, f_C / M_C\right) dt} \quad (1)$$

In the equation above, $\Phi(t)$ represents the flow of gasses in mol/s, $\Phi_{\text{m,oil}}(t)$ the oil feed rate in kg/s, $f_C$ the mass fraction of carbon in pyrolysis oil, and $M_C$ is the molar mass of carbon. $\tau_d$ is the delay (dead) time between the reactor and the gas analysis equipment. The delay was measured by gas pulse injection experiments which showed plug-flow behavior.

Carbon that was deposited on the bed material is not included in this $\zeta_{\text{C to gas.}}$ In order to measure the amount of deposited carbon air was used to burn off the carbon in the case of the oil gasification experiments. If a redox experiment was performed, carbon was (partly) oxidized via reactions (3) and (6) (Table 1). In both cases CO and $CO_2$ was formed, which was included in the total carbon conversion balance, $\zeta_{\text{C total.}}$ $\zeta_{\text{C total}}$ is $\zeta_{\text{C to gas}}$ plus the amount of carbon (coke) deposited on the bed material and is used for the mass balance closure evaluation of the experiments.

$$\zeta_{\text{C total}} = \zeta_{\text{C to gas}} + \frac{\int_{t_{\text{start air/N}_2\text{ injection}}+\tau_d}^{t_{\text{end air/N}_2\text{ injection}}+\tau_d} \left(\Phi_{CO}(t) + \Phi_{CO_2}(t)\right) dt}{\int_{t_{\text{start oil injection}}}^{t_{\text{end oil injection}}} \left(\Phi_{\text{m,oil}}(t)\, f_C / M_C\right) dt} \quad (2)$$

The momentary oxygen balance, $\zeta_{\text{O to gas}}(t)$, defined as the amount of oxygen transferred from the pyrolysis oil to gaseous products, is a measure for the degree of reduction at a certain time in the reduction step. If the gases initially produced by gasification of pyrolysis oil reduce the iron oxides, the amount of oxygen in the product gas will be higher than the amount of oxygen fed in pyrolysis oil. Unfortunately it was not possible to measure the water content of the produced gasses online. Therefore, the $\zeta_{\text{O to gas}}$ used here is only indicative and was used qualitatively for, e.g., the comparison between inert and catalytic experiments.

$$\zeta_{\text{O to gas}}(t) = \frac{\Phi_{CO}(t+\tau_d) + 2\Phi_{CO_2}(t+\tau_d)}{\Phi_{\text{m,oil}}(t)\, f_O / M_O} \quad (3)$$

In Eq. (3), $f_O$ is the mass fraction of oxygen in pyrolysis oil (including water). Graphs containing $\zeta_{\text{O to gas}}(t)$ were smoothened with the adjacent average method, in which the smoothed value at index $i$ is the average of the data points (with $n = 5$) in the interval $[i - (n-1)/2,\ i + (n-1)/2]$, inclusive.

Gas productions during gasification, reduction or oxidation are calculated as follows (example hydrogen production during reduction):

$$H_2 = \frac{\int_{t_{\text{start reduction}}+\tau_d}^{t_{\text{end reduction}}+\tau_d} \Phi_{H_2}(t)\, dt \cdot (R_{\text{gas}} T/P)}{\int_{t_{\text{start oil injection}}}^{t_{\text{end oil injection}}} \Phi_{\text{m,oil}}(t) \cdot (1 - X_{\text{m,H}_2O})\, dt} \quad (\text{Nm}^3/\text{kg dry oil}), \quad (4)$$

in which $X_{\text{m,H}_2O}$ is the water fraction in the pyrolysis oil, and $T$ and $P$ are defined at normal conditions (273 K and 1 bar).

In the reduction experiments pyrolysis oil is sprayed over a fluidized batch of $Fe_3O_4$. How much of this initially present iron oxide can be reduced, obviously depends on the amount of pyrolysis oil injected. However, the amount of $Fe_3O_4$ reduced is expected not to be linearly proportional to the amount of pyrolysis oil injected, as it has been reported by several researchers [19] that the reduction rate depends on the conversion level of the $Fe_3O_4$ particles. By evaluating the hydrogen production in the oxidation step per unit injected pyrolysis oil as a function of the amount $Fe_3O_4$ initially present per unit injected pyrolysis oil, an indication is obtained on the optimal iron oxide circulation rate (kg $Fe_3O_4$/s/kg oil/s) of the looping concept. To evaluate the total redox cycle the integral ($R$) was used.

$$R = \frac{\text{Fe}_3\text{O}_4\text{ initially present}}{\int_{t_{\text{start oil injection}}}^{t_{\text{end oil injection}}} \Phi_{\text{m,oil}}(t)\, dt} \quad (5)$$

$1/R(t)$, which is proportional to the runtime of the reduction, was used to discuss the momentary reduction rate during a single reduction test:

$$\frac{1}{R(t)} = \frac{\int_{t_{\text{start oil injection}}}^{t} \Phi_{\text{m,oil}}(t)\, dt}{\text{Fe}_3\text{O}_4\text{ initially present}} \quad (6)$$

#### 3.4.2. Oxidation

The amount of oxygen that is removed from the iron oxide during the reduction, $\Delta O_{\text{iron oxide}}$ (mol), is calculated from the

hydrogen produced in the oxidation step via reactions (2) and (4) (Table 1) and corrected for hydrogen produced from char gasification reactions in the oxidation step, reactions (7) and (8) (Table 1).

$$\Delta O_{\text{iron oxide}} = \int_{t_{\text{start steam injection}}+\tau_d}^{t_{\text{end steam injection}}+\tau_d} (\Phi_{H_2}(t) - \Phi_{CO}(t) - 2\Phi_{CO_2}(t))\,dt \quad (\text{mol}) \tag{7}$$

On the basis of $\Delta O_{\text{iron oxide}}$ the conversion of iron oxide is calculated as follows:

$$\alpha(Fe_3O_4{-}Fe) = \frac{\Delta O_{\text{iron oxide}}}{S_0} \times 100 \quad (\%) \tag{8}$$

In which $S_0$ is the amount of oxygen (mol) initial present in $Fe_3O_4$ in the fluidized bed.

The water conversion during oxidation with steam, which is equal to the amount of hydrogen produced in this step, is defined as:

$$\zeta_{H_2O}(t) = \frac{\Phi_{H_2O,in}(t) - \Phi_{H_2O,out}(t+\tau_d)}{\Phi_{H_2O,in}(t)} = \frac{\Phi_{H_2}(t+\tau_d)}{\Phi_{H_2O,in}(t)} \tag{9}$$

The steam converted to hydrogen by the conversion of carbon (reactions (7) and (8)) during oxidation is defined as:

$$\zeta_{H_2O\,\text{reacted with C}}(t) = \frac{\Phi_{CO}(t+\tau_d) + 2\times\Phi_{CO_2}(t+\tau_d)}{\Phi_{H_2O,in}(t)} \tag{10}$$

A similar ratio $R_{ox}$ during the oxidation as during reduction ($R$) is defined:

$$R_{ox} = \frac{Fe_3O_4\,\text{initially present}}{\int_{t_{\text{start }H_2O\text{ injection}}}^{t_{\text{end }H_2O\text{ injection}}} \Phi_{m,H_2O}(t)\,dt} \tag{11}$$

In which the $\Phi_{m,H_2O}$ is the flow of water added to the system in kg/s. Also in this case, the inverse of the momentary $R_{ox}$ is used to evaluate the oxidation rate during a single oxidation step.

$$\frac{1}{R_{ox}(t)} = \frac{\int_{t_{\text{start }H_2O\text{ injection}}}^{t} \Phi_{m,H_2O}(t)\,dt}{Fe_3O_4\,\text{initially present}} \tag{12}$$

## 4. Results

### 4.1. Mass balances

A maximum carbon recovery ($\zeta_{C\ \text{total}}$) of 80% was obtained; thus 20% of the carbon in the feed was not recovered in the experiments. Similar low carbon to gas conversions with pyrolysis oil were observed by Panigrahi et al. [22] and Van Rossum et al. [26] who found a conversion of biomass derived oil to the gas phase of 81% at 800 °C. After the gasification experiments coolers and other cold parts in the set-up that were in contact with the gas effluent were contaminated with carbonaceous compounds (liquid and solid). A small fraction of the cokes particles that were formed could be separated with the cyclone (1–2% of the C input). Also 1–2 wt.% of the carbon input was likely converted to tar [26]. The effect of spraying a cold pyrolysis oil into a hot fluidized bed probably caused formation of highly porous carbon structures which pass through the set-up and were not detected with the analysis methods used [27].

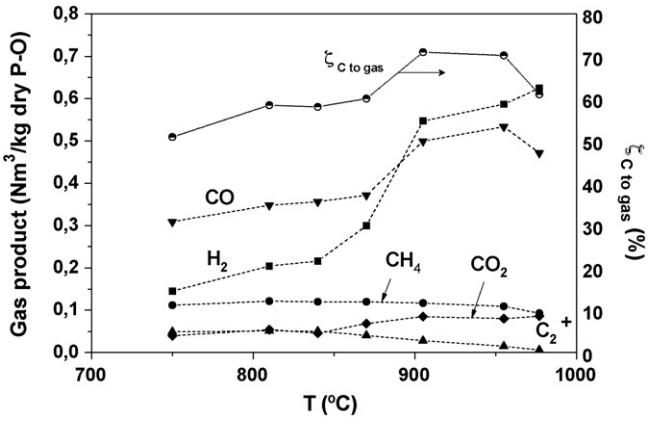


Fig. 5. Pyrolysis oil gasification in the fluidized sand bed: gas production and carbon to gas conversion ($\zeta_{C\ \text{to gas}}$) at different reaction temperatures.

### 4.2. Gasification of pyrolysis oil over a fluidized sand bed

Gasification was conducted at different temperatures between 750 and 970 °C. A constant gas composition in time was observed and maintained for about 45 min. The carbon conversion of the pyrolysis oil to the gas phase, which is a measure of the overall conversion of pyrolysis oil to the gas phase, increased from 51% at 750 °C to 70% at 900 °C after which it leveled off to 950 °C (see Fig. 5). A decrease in $\zeta_{C\ \text{to gas}}$ was observed at a temperature of 970 °C. On average, around 5.1% of the carbon in the pyrolysis oil deposited on the sand particles, independent of the temperature.

An overview of the measured gas production from the gasification of pyrolysis oil as a function of the reactor

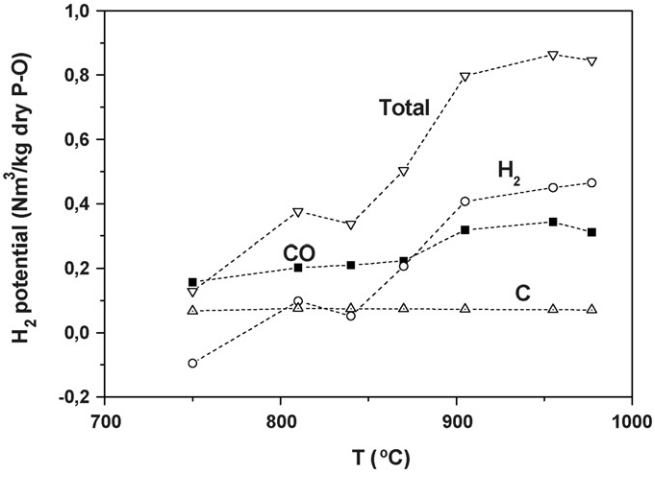


Fig. 6. Calculated hydrogen production potential in the steam-iron process with gasified pyrolysis oil. Experimental data of gasified pyrolysis oil (see Fig. 5) is combined with equilibrium data of the reduction of magnetite to wustite with C, CO and $H_2$.

temperature is shown in Fig. 5. Important for the reduction of iron oxide with pyrolysis oil is the formation of CO and $H_2$. The production of these reducing compounds by gasification of pyrolysis oil increased with increasing temperature. This can be ascribed to the increase in carbon conversion, reforming of $C_2^+$ compounds above 850 °C, and probably the water–gas-shift reaction. Methane production was not affected by the reactor temperature. The measured gas production as given in Fig. 5 is used to estimate the amount of pure hydrogen than can be produced from pyrolysis oil via the steam-iron process (see Fig. 6) if the iron oxide used has no catalytic activity for reforming of $C_xH_y$, gasification of coke and the water–gas-shift. For this estimate, the chemical equilibrium of the produced gases and solid carbon (in the fluidized sand bed) with $Fe_3O_4/Fe_{0.945}O$ is calculated at the reactor temperature, which yields the maximal amount of $Fe_{0.945}O$ that can be produced from $Fe_3O_4$ per kg pyrolysis oil in the reduction. This amount of $Fe_{0.945}O$ then gives the hydrogen production (per kg pyrolysis oil) in the oxidation step by assuming that the oxidation of $Fe_{0.945}O$ with steam is complete. These calculations predict that the hydrogen production at the foreseen process temperature of 810 °C is 0.37 N $m^3$ per kg dry pyrolysis oil when non-catalytic iron oxide is used. In the section ''hydrogen production and potential'' this predicted hydrogen production level will be compared with results obtained from redox cycle experiments.

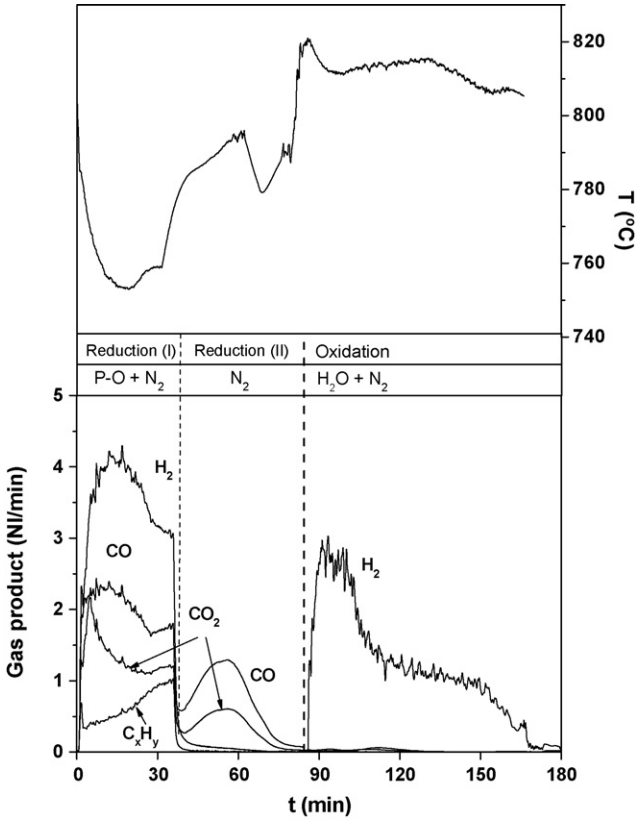


Fig. 7. Gasses produced and fluidized bed temperature during a redox cycle with pyrolysis oil (P-O) and BIC iron oxide. The presented temperature is the average temperature over the bed material.

Table 6
Gas products from redox cycle (first cycle with BIC iron oxide) with 314 g pyrolysis oil and 1.75 kg $Fe_3O_4$

| | Reduction (I) | Reducation (II) | Oxidation |
|---|---|---|---|
| Temperature | 754 | 761 | 810 |
| Total average gas production (N $m^3$/kg dry pyrolysis oil) | | | |
| $H_2$ | 0.57 | – | 0.53 |
| CO | 0.32 | 0.14 | 0.01 |
| $CO_2$ | 0.22 | 0.06 | 0.01 |
| $CH_4$ | 0.07 | – | – |
| $C_2^+$ | 0.02 | – | – |
| $\zeta_{C\ to\ gas}$ | 59.9 | | |
| $\zeta_{C\ total} - \zeta_{C\ to\ gas}$ | | 19.0 | |
| Other | | | |
| $\zeta_{H_2O}(t)_{t=90-100}$ | | 69.9% | |
| $\zeta_{H_2O}(t)_{t=110-150}$ | | 29.0% | |
| $\alpha(Fe_3O_4–Fe)$ | | 15.3% | |

### 4.3. Gasification of pyrolysis oil over an iron oxide bed

Below, a redox cycle (first cycle) using BIC iron oxide is described in detail. In Fig. 7 the gas production of the product gas during this cycle is given versus the running time of the experiment. The temperature is also presented with the running time of the experiment (a short period of decrease in temperature between 70 and 75 min was caused by an external experimental problem). Table 6 lists time averaged results of this test. The starting temperature was set at 802 °C (set-point).

#### 4.3.1. Reduction

From 0 to 35 min, pyrolysis oil was injected with a constant flow rate. Contrary to the sand bed experiments no constant gas production was observed during pyrolysis oil injection. Most striking was the decrease of $CO_2$ during the first 15 min of injection, which points towards a decrease in the rate of the reduction reaction of $Fe_3O_4$ with CO. The production of hydrogen was high during reduction step I (see Fig. 7): on average 0.57 $H_2$ N $m^3$/kg dry pyrolysis oil compared with 0.21 $H_2$ N $m^3$/kg dry pyrolysis oil over the fluidized sand bed (compare Tables 6 and 8). Probably reforming reactions of $C_xH_y$ were enhanced by the BIC iron oxide, resulting in lower $CH_4$ and $C_2^+$ production and higher CO and $H_2$ production. After 20 min of pyrolysis oil injection, the catalytic activity of the iron oxide decreased resulting in a higher $C_xH_y$ production and lower CO and $H_2$ production. This decrease in catalytic activity could be due to the change of oxidation state of the iron oxide, but also by the deactivation due to carbon deposition on the particles. The gas produced during the reduction has a good $H_2$/CO ratio (2:1) for further upgrading to a synthesis gas. The composition of this gas is dependent on the water content of the oil. Higher $H_2$/CO ratios were found with a higher water content of the oil. The temperature during pyrolysis oil injection dropped over a period of about 15 min, which after a slow increase in temperature was observed. When stopping the oil injection an increase towards the set-point was measured.

Carbon (coke) deposition can be clearly shown from the second part of the reduction (35–85 min) in which only nitrogen

Table 7
Equilibrium oxidation data $T = 810$ °C

| Reaction | $\zeta_{H_2O}$ |
|---|---|
| $3.17Fe_{0.945}O$ (s) + $0.83H_2O \leftrightarrow Fe_3O_4$ (s) + $0.83H_2$ | 40.7% |
| Fe (s) + $H_2O \leftrightarrow FeO$ (s) + $H_2$ | 66.3% |

was injected. In this second part of the reduction, the coke that was deposited during pyrolysis oil injection is still reacting with the iron oxide producing CO, $CO_2$, and some $H_2$. It can be calculated that a total of 19% of the carbon input was reacting in this second part of the reduction resulting in an $\alpha(Fe_3O_4–Fe)$ of 8.7%. For the total reduction period an $\alpha(Fe_3O_4–Fe)$ of 15.3% was calculated. This means that more than half of the total reduction with pyrolysis oil was due to deposited coke on the iron oxide. The $CO/CO_2$ ratio of 2.2 found in the second part was high enough for the reaction of wustite to metal iron to take place.

#### 4.3.2. Oxidation

At the start of the oxidation a high $H_2$ production rate was obtained (3 l/min), decreasing to 1.1 l/min. At the maximum, $t = 90$–100 min, about 70% of the steam was converted to hydrogen, reducing to roughly 30% between $t = 110$ and 150 min. The initial high conversion of steam could not be caused (based on thermodynamics) by the reaction of wustite with steam (see Table 7). Probably metal iron was formed resulting in a higher conversion of steam. The measured conversion of steam is higher than the expected conversion based on thermodynamics for the reaction of metal iron to wustite. This might be caused by the additives like chromium and copper oxides in the BIC iron oxide. It can therefore be concluded that, in general, the metal iron is initially oxidized to wustite followed by the oxidation of wustite to magnetite. A low reduction degree of the iron oxide was calculated ($\alpha = 15.3\%$), so metal iron was not expected. Because of this low conversion, it is likely that metal iron is formed on the surface while unreacted $Fe_3O_4$ is still present in the centre of the particle. The temperature rose above the set-point when the oxidation was started. During the oxidation of wustite an increase of 10 degrees Celsius above the set-point was found.

After analyzing the first two redox cycles it was observed that the reduction is slow at an $R$-ratio (kg $Fe_3O_4$/kg pyrolysis oil) below 15. Therefore, subsequent redox cycles with fresh material were performed until a total ratio of minimum 15 was obtained. In these experiments carbon deposition was lower: on average 11% of the total carbon input (from 100 g of oil).

### 4.4. Repeated cycling

To investigate the deactivation of the iron oxides, several cycles were performed with the iron oxide (13 cycles with BIC and 4 cycles with BF). Figs. 8 and 9 show the momentary $\zeta_{O\ to\ gas}(t)$ during the pyrolysis oil injection as a function of the amount of oil injected ($1/R(t)$). Clearly at similar temperature, the reduction activity of BF iron oxide is lower than the reduction activity of BIC iron oxide. This could be caused by additives in the BIC iron oxide which facilitate the reduction rate of the iron oxide. Furthermore the gasses formed from the oil during reduction with both iron oxides differed substantially. The BIC iron oxide, as indicated in the previous paragraph, clearly showed an activity in catalyzing reforming reactions of $C_xH_y$, resulting in an increased formation of $H_2$ and CO. This was not the case for tests with BF iron oxide in which a gas composition similar to gasified oil over the sand bed was obtained. The results of a typical redox cycle with BF iron oxide compared to results obtained with sand are presented in Table 8. The high $CO/CO_2$ ratio of 3 indicates that not the full reduction potential of the oil was used.

For both iron oxides the amount of oxygen transported to the gas phase ($\zeta_{O\ to\ gas}(t)$) decreased over the subsequent cycles and

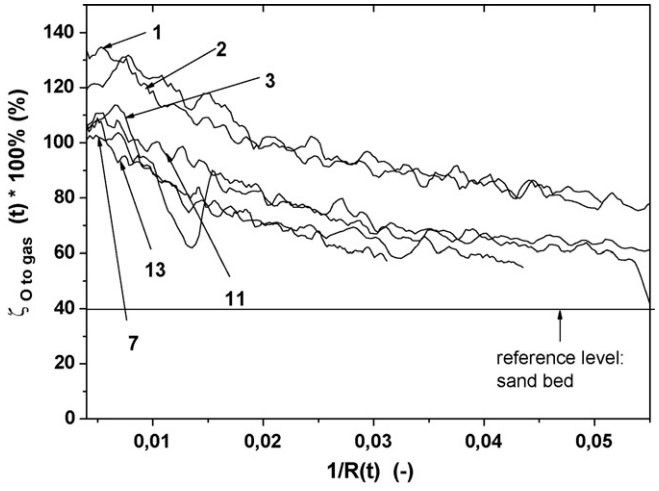


Fig. 8. $\zeta_{O\ to\ gas}$ vs. $1/R(t)$ for repeated cycling of BIC iron oxide during reduction. In all experiments the reduction temperature was in the range of 745–755 °C. The $1/R(t)$ on the $x$-axis represents the increasing oil:$Fe_3O_4$ ratio during oil injection. The horizontal line represents a reference for oil gasification over an inert sand bed obtained at 800 °C.

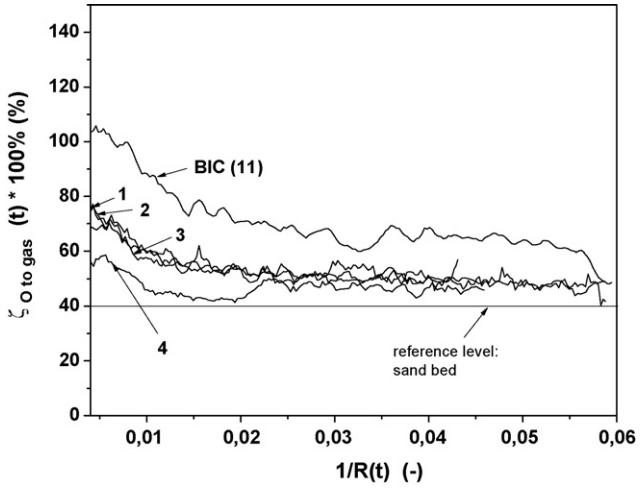


Fig. 9. $\zeta_{O\ to\ gas}$ vs. $1/R(t)$ for repeated cycling of BF iron oxide compared to BIC iron oxide during reduction. In all experiments the reduction temperature was in the range of 745–755 °C. The $1/R(t)$ on the $x$-axis represents the increasing oil:$Fe_3O_4$ ratio during oil injection. The horizontal line represents a reference for oil gasification over an inert sand bed obtained at 800 °C.

Table 8
Gas products from redox cycle (first cycle with BF iron oxide) with 100 g pyrolysis oil and 1.7 kg $Fe_3O_4$

| | BF | | | Sand |
|---|---|---|---|---|
| | Reduction (I) | Reduction (II) | Oxidation | |
| Temperature | 780 | 800 | 820 | |
| Total average gas production (N $m^3$/kg dry pyrolysis oil) | | | | |
| $H_2$ | 0.20 | | 0.25 | 0.20 |
| CO | 0.33 | 0.03 | 0.003 | 0.35 |
| $CO_2$ | 0.11 | 0.04 | 0.01 | 0.04 |
| $CH_4$ | 0.14 | – | – | 0.12 |
| $C_2$+ | 0.05 | – | – | 0.05 |
| $\zeta_{C\ to\ gas}$ | 57.1 | | | 58.4 |
| $\zeta_{C\ total} - \zeta_{C\ to\ gas}$ | | 6.7 | | |
| Other | | | | |
| $\zeta_{H_2O,max}$ | | 22% | | |
| $\alpha(Fe_3O_4–Fe)$ | | 2.2% | | |

The gas products obtained with the cracking of the oil over a sand bed at 810 °C is also presented.

consequently the reduction rate during these cycles was decreasing. Most of the deactivation for the BIC iron oxide took place in the first two redox cycles. The patterns of cycle 7, 11 and 13 of BIC iron oxide were similar indicating that the activity of the iron oxide approaches a steady state. In all cycles for both iron oxides the reduction rate is optimal at $1/R(t)$ values <0.01. Apparently, the reduction rate is high when the particle consists of $Fe_3O_4$ and decreases when the particle is only partly reduced. This has also been acknowledged in literature [28]. At high $1/R(t)$ values (>±0.04) most of the gases produced by gasification of pyrolysis oil pass through the bed unconverted. This can be concluded because above a $1/R(t)$ value of 0.04 about the same amount of oxygen is found in the gas phase as in the pyrolysis oil gasification experiments over the fluidized sand bed (see Figs. 8 and 9).

The difference in activity between BF and BIC material was also evident from the steam conversion in the oxidation step.

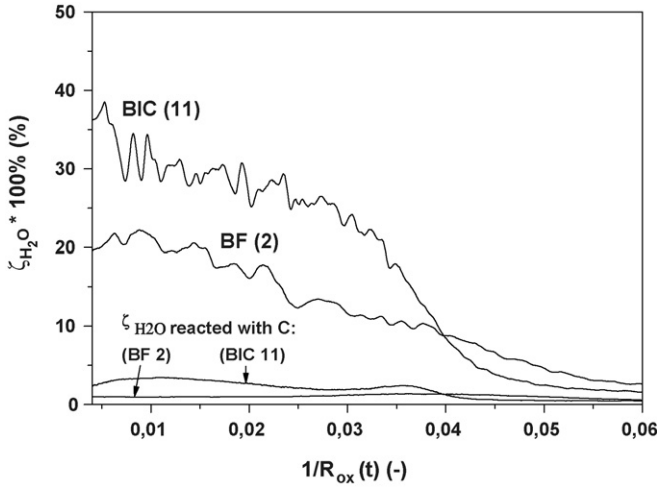


Fig. 10. Total momentary $H_2O$ conversion during oxidation at $T = 810$ °C of reduced BIC and BF iron oxide (Fig. 9). $\zeta_{H_2O\ reacted\ with\ C}$ of BF and BIC is the conversion of $H_2O$ by the reaction with deposited carbon.

Fig. 10 shows that the oxidation activity of BF iron oxide was lower than the BIC iron oxide. The equilibrium value of 40.7% steam conversion at 810 °C was almost reached with the BIC iron oxide (see Table 7). Both iron oxides showed a steady steam conversion over a wide range of $1/R_{ox}(t)$. Fig. 10 also shows that, apparently, carbon remained on the iron oxide after the reduction resulting in a water–gas reaction ($\zeta_{H_2O\ reacted\ with\ C}$) in the oxidation step.

The purity of the hydrogen produced in the oxidation step depends on the conversion of deposited carbon in the reduction step. The reduction of iron oxide with carbon deposits can take place above temperatures of 700 °C. Complete conversion of the carbon, depends on temperature, amount of carbon deposits and the time between the end of oil injection and start of the oxidation. A high purity hydrogen (99 vol.%) could be obtained when these three factors were taken into account.

### 4.5. Deactivation

During the redox cycles with the BIC iron oxides a deactivation was observed in the first 3 cycles, which was less severe in the case for the BF iron oxide. BET analyses of the BIC iron oxide showed a substantial decrease in surface area of the BIC particles as given in Table 9. A worsening of the surface area of BIC iron oxide is observed after a reduction with $H_2$ of fresh material ($Fe_2O_3$) to metal iron. Therefore, the decrease in surface area observed when redox cycles were performed could have partly been caused by the first reduction of fresh material to a lower oxide.

It was found that after 3 cycles the pore structure, which was accessible for the evaluation gas, had deteriorated. Only the outer surface of the particles seemed to contribute to the BET surface area. The decrease in surface area between the 3rd and 14th cycle was less severe. The activity of the BF iron oxide was also influenced by the redox cycles performed. The BF iron oxide has a lower surface area to begin with (see Table 3) and therefore further decrease is probably slower than in the case with the BIC iron oxide.

From the oxygen balances during the injection of the pyrolysis oil it was found that high $Fe_3O_4$/pyrolysis oil ratios were optimum. This optimum ratio was increased after more redox cycles with pyrolysis oil were performed. So the time, in which a high reduction rate was anticipated, decreased when the iron oxide deactivated. A high reduction rate was expected at the start of the reduction when the particle consists of $Fe_3O_4$. When the outer surface of the particle was reduced a boundary layer with reduced species was formed, which most likely

Table 9
BET surface area analysis of BIC iron oxide after reduction with $H_2$ and redox cycles with pyrolysis oil

| | BET analysis ($m^2$/g) | Fraction $d_p$ >225 um |
|---|---|---|
| $Fe_2O_3$ ($d_p$ = 1.0 mm) | 31.12 | 100% |
| Fe ($Fe_2O_3$ fully reduced with $H_2$ at 800 °C) | 4.67 | 100% |
| After 3 cycles | 0.76 | 51% |
| After 14 cycles | 0.37 | |

shows a slowing down of the reduction reaction [3,29]. Probably already in the first cycle boundary layer formation had an effect on the reduction rate, but this effect was enhanced with repeated cycling. This was observed for both the reduction with pyrolysis oil and ethanol in which very little carbon formation on the surface was observed after injection. This also confirms that the decrease in rate is probably caused by changes in the iron oxide structure and not by the formation of carbon on the surface. Due to the wustite boundary layer the reaction rate is slowed down and can be limited by diffusion processes in the solid [30–32].

SEM pictures were taken to study the outer surface of the particles. The first picture (Fig. 11A) shows the outer surface of unused BIC iron oxide particle, where a high surface area was observed. The second picture (Fig. 11B) is the surface of deactivated BIC iron oxide area after 3 redox cycles. A less porous structure is observed as expected from the BET analysis. Fig. 11C shows a sintered structure with greatly enhanced grain size that was obtained after 14 redox cycles. The BIC material contains some copper oxide (2.7 wt.%) which are seen to form crystals on the surface after 14 cycles (Fig. 11C). Copper oxide is expected to be more reactive for reduction from a thermodynamic point of view. This copper oxide on the surface might have an effect on the high reduction rate at the start of the reduction reaction [33].

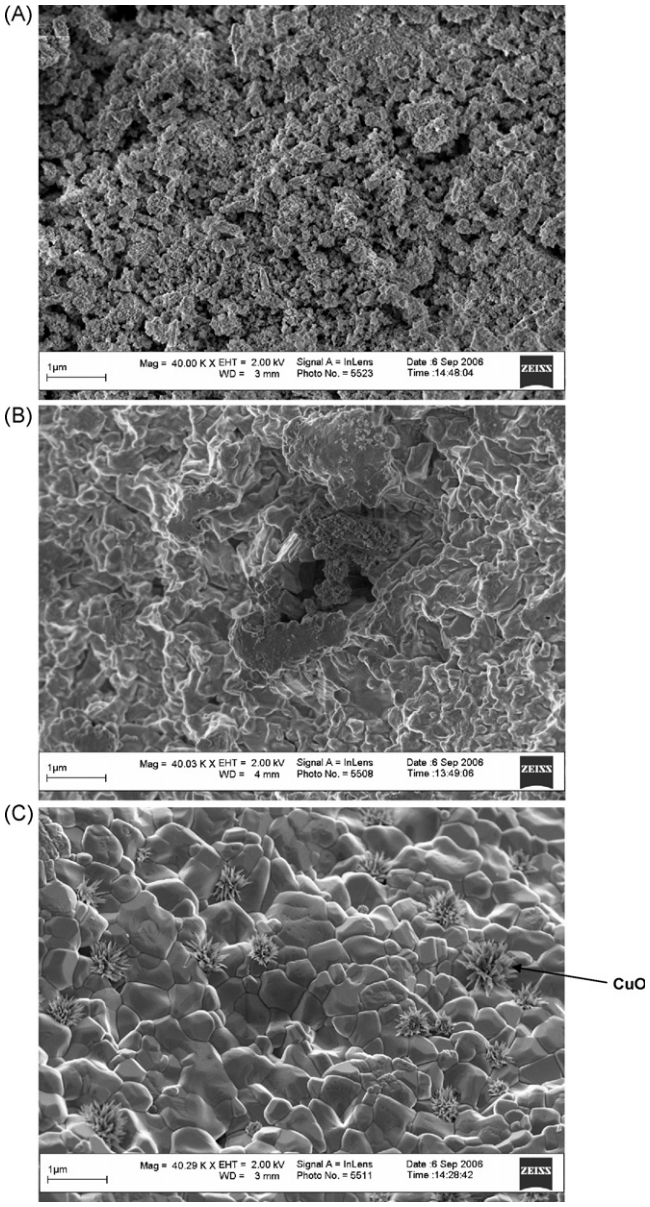


Fig. 11. Surface area of BIC iron oxide. (A) Fresh iron oxide ($Fe_2O_3$). (B) After 3 redox cycles ($Fe_3O_4$). (C) After 14 redox cycles ($Fe_3O_4$), copper oxide crystals are formed on the surface.

An interesting point was the rapid morphological changes in the porous iron particles. Intensive recycling giving rise to substantial internal self diffusion in the iron oxide seemed to speed up densification and sintering. This internal morphological change did affect the availability of iron oxide for the steam-iron process but not to the extent of the BET surface area reduction. Large cracks in the particle were observed in the fresh material and were still present in the material after 14 cycles (Fig. 12). These cracks make it possible for gasses to migrate in and out of the particles that could explain the relatively high activity after deactivation.

Deactivation caused by the sintering of the surface during repeated cycling was also observed by other researchers. It was reported that the stability could be improved by using additives like Al, Mo, Ce and Cr [34,35] or quartz [36] in the iron oxide. Furthermore, if only the outer layer of the iron oxide is highly reactive, iron oxide can be deposited on a porous carrier, which could prevent severe sintering of the iron oxide particle.

Other factors, like the swelling and shrinking of the iron oxide due to the change of the crystal structure, agglomeration and break-up of the particles play a role in the deactivation of the particles in the fluidized bed set-up. The complex deactivation and the influence of this deactivation on the use of pyrolysis oil in the steam-iron process will be further studied in more detail.

### 4.6. Hydrogen production and potential

The hydrogen production in the redox cycle was measured from the results obtained in the experimental set-up with BF and BIC iron oxides. It was already observed that the reduction reaction was very rapid and slowed down when a small part of

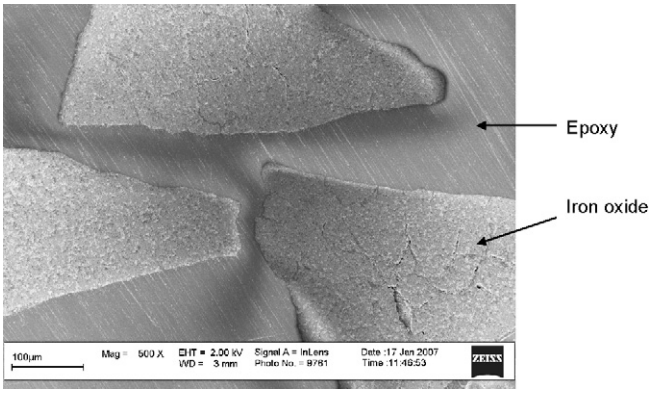


Fig. 12. Cross-section BIC iron oxide after 14 redox cycles ($Fe_3O_4$).

Table 10
Gas product of the gas products in a redox cycle with BIC and BF iron oxide with high $Fe_3O_4$/oil (=*R*) ratio

| | BIC | | BF | |
|---|---|---|---|---|
| *R* | 148.3 | | 157.4 | |
| *T* (°C) | 780 | | 795 | |
| | Reduction | Oxidation | Reduction | Oxidation |
| Gas product (N $m^3$/kg dry oil in) | | | | |
| $H_2$ | 0.32 | 0.84 | 0.22 | 0.43 |
| $C_xH_y$ | 0.05 | | 0.13 | |
| CO | 0.26 | 0.002 | 0.27 | 0.002 |
| $CO_2$ | 0.46 | 0.005 | 0.26 | 0.008 |
| $CO/CO_2$ (mol/mol) | 0.57 | | 1.04 | |
| Other | | | | |
| LHV gas product (MJ/N $m^3$ gas product) | 7.8 | 10.6 | 11.7 | 10.5 |
| $\eta$ based on LHV (MJ gas produced/MJ oil in) | 0.38 | 0.40 | 0.46 | 0.20 |
| $\alpha(Fe_3O_4$–Fe) | | 1.0 | | 0.5 |

the particle was reduced. Therefore, experiments with *R* values of 150 down to 15 were performed (Fig. 13). From this figure an internal circulation (kg/s)/feed rate (kg/s) ratio of 100 for both iron oxides seems optimum for the conversion of pyrolysis oil to hydrogen. This ratio is comparable to conventional CFB biomass gasification, where sand is circulated for heat transfer. In this process a circulation rate (*R*) of 50 sand kg/s/dry biomass (kg/s) is appropriate [37].

The highest hydrogen product (from the oxidation) that was obtained with the BF iron oxide was 0.35 $H_2$ N $m^3$/kg dry pyrolysis oil, which comes close to the expected value of 0.37 $H_2$ N $m^3$/kg dry pyrolysis oil from gasified pyrolysis oil over the sand bed at 810 °C (see Fig. 6). It can therefore be concluded that the conversion of pyrolysis oil to reducing gasses was not influenced to a large extend by the BF iron oxide. The gas produced in the reduction step still had a reducing capacity even at high *R* values (Table 10). This was found by comparing the $CO/CO_2$ ratio obtained with the expected equilibrium value. If this remaining CO would also be used for reduction an additional hydrogen production of 0.07 N $m^3$/kg dry pyrolysis oil could be obtained.

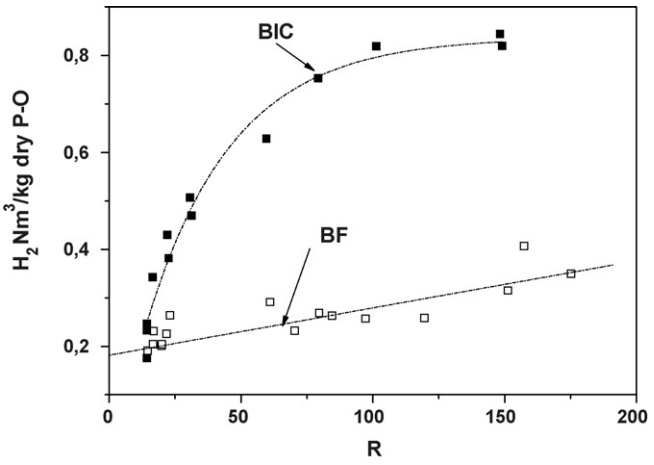


Fig. 13. Hydrogen produced in the oxidation step from oxidized iron oxide with steam (corrected for water gas reaction). After initial reduction with an *R* value between 15 and 100 at temperatures between 810 and 750 °C. Deactivated BIC iron oxide is used in this graph (cycle number 5–13) and BF iron oxide cycle number (1–15).

The BIC iron oxide has a twice as high hydrogen production at high *R* values than expected from the calculated hydrogen production from gasified pyrolysis oil. This is caused by the catalytic activity of the iron oxide for reforming reactions, resulting in more $H_2$ and CO during the gasification of the pyrolysis oil. The highest hydrogen production of 0.84 N $m^3$/kg dry pyrolysis oil in the set-up was obtained with the BIC iron oxide and an *R* value of 100 kg $Fe_3O_4$/kg pyrolysis oil or higher. The found $CO/CO_2$ ratio of 0.57 in the reduction step at high *R* values was lower than the equilibrium value of 0.65 at 780 °C (Table 10). This shows that a high conversion of CO in the reduction was obtained. A lower $CO/CO_2$ value found than expected from the thermodynamic data and reaction between wustite and magnetite might indicate that the additives in the BIC iron oxide (mainly copper and chromium oxide) probably had an effect in the established $CO/CO_2$ ratio. The maximum attainable hydrogen production from pyrolysis oil with the steam-iron process can be calculated from thermodynamics: this value is 1.16 N $m^3$/kg dry pyrolysis oil at 800 °C. In this calculation, first the equilibrium between pyrolysis oil (in the form of $C_xH_yO_z$, see Table 2) and $Fe_3O_4/Fe_{0.945}O$ was calculated while assuming that there was an excess of $Fe_3O_4$ and that at equilibrium the following gases could be present: CO, $CO_2$, $CH_4$, $H_2$, and $H_2O$. This gives the amount of $Fe_{0.945}O$ formed per kg pyrolysis oil, on basis of which the amount of $H_2$ was calculated by assuming complete conversion in the oxidation with steam to $Fe_3O_4$.

## 5. Conclusion

Pyrolysis oil was used successfully as a reducing agent in the steam-iron process. The most important findings from the experiments performed are listed below:

1. A significant amount of relatively pure hydrogen can be produced in a redox cycle with iron oxides, next to a fuel gas. The use of a catalytic iron oxide resulted in an improved

conversion of pyrolysis oil to pure hydrogen, due to the enhanced reforming of hydrocarbons in the reduction step.
2. Directly injecting pyrolysis oil in a fluidized bed of iron oxides had the particular advantage that deposited carbon on the iron oxides contributed to the reduction of iron oxides. Pure hydrogen can only be obtained when the reduction with this deposited carbon is completed.
3. Overall performance of the process is optimal when thermodynamic equilibrium in the gas phase is obtained during reduction. This was achieved by increasing the iron oxide to pyrolysis oil ratio that corresponds to a high circulation rate of iron oxides and low conversion of the iron oxide particle. An additional advantage of a high circulation rate is an improved heat transport in the fluidized bed, needed for the cold pyrolysis oil injection during the endothermic reduction.
4. Both iron oxides showed potential to use in the production of hydrogen from pyrolysis oil in the proposed concepts. The BF iron oxide is more suitable for a once-through concept. The BIC iron oxide can be used in a cycling process, though further improvements of the material should enhance the stability and activity.
5. Deactivation of the iron oxide was observed, causing a decrease in reaction rate during reduction. Observed loss of surface area of the particles with BET and SEM analysis could partly explain this deactivation. More research is necessary to understand the deactivation process of the iron oxide.

## Acknowledgements

The authors gratefully acknowledge the funding support within the Sustainable Hydrogen Programme of ACTS/NWO in the Netherlands. Thanks to B. Ataoglu for performing part of the experiments.

## References

[1] P.R. Ramage, R. Agrawal, The Hydrogen Economy: Opportunities, Costs, Barriers and R&D Needs, National Academies Press, Washington, DC, 2004.
[2] J. Huffman, Chemical Market Reporter, 267 (2005) 18.
[3] F. Oeters, Ullmann's Encyclopedia of Industrial Chemistry; Iron, seventh ed., John Wiley & Sons, New York, 2006.
[4] A. Raissi, D.L. Block, IEEE Power Energy Mag. 11/12 (2004) 40.
[5] M. Groeneveld, Personal Communication, Shell, 2006.
[6] M.J.A. Tijmensena, A.P.C. Faaij, C.N. Hamelinck, M.R.N. Hardeveld, Biomass Bioenergy 23 (2002) 129.
[7] M.J. Prins, Fuel Process. Technol. 86 (2004) 375.
[8] M.C. Samaloda, W. Baldauf, I.A. Vasalos, Fuel 14 (1998) 1667.
[9] C.N. Hamelinck, A.P.C. Faaij, J. Power Sources 111 (2002) 1.
[10] W. Iwasaki, Int. J. Hydrogen Energy 28 (2003) 939.
[11] A.V. Bridgwater, Fast Pyrolysis of Biomass: A Handbook, vol. 2, CPL Press, Newbury, 2002.
[12] A.V. Bridgwater, Therm. Sci. 8 (2004) 21.
[13] Gmelin, eighth ed., Gmelins Handbuch der Anorganischen Chemie; Wasserstoff, vol. 2, Verlag Chemie, Leipzig, 1927, p. 30.
[14] P.B. Tarman, Proc. 5th Synth. Pipeline Gas Symposium, Chicago, Illinoism, 29–31 October, (1973), p. 114.
[15] P.B. Tarman, Proc. 10th Synth. Pipeline Gas Symposium, Chicago, Illinois, 31 October–2 November, (1978), p. 235.
[16] S. Fukase, T. Suzuka, Can. J. Chem. Eng 72 (1994) 272.
[17] S. Fukase, T. Suzuka, Appl. Catal. A 100 (1993) 1.
[18] V. Hacker, J. Power Sources 118 (2003) 311.
[19] V. Hacker, R. Fankhauser, G. Faleschini, H. Fuchs, K. Friedrich, M. Muhr, K. Kordesch, J. Power Sources 86 (2000) 531.
[20] T. Mattisson, A. Lyngfelt, Proc. 2nd Nordic Minisymposium on Carbon Dioxide Capture and Storage, Göteborg, 26 October, (2001), p. 46.
[21] L. Garcia, R. French, S. Czernik, E. Chornet, Appl. Catal. A 201 (2000) 225.
[22] S. Panigrahi, A.K. Dalai, S.T. Chaudhari, N.N. Bakhshi, Energy Fuels 17 (2003) 637.
[23] T. Mattisson, A. Lyngfelta, P. Chob, Fuel 80 (2001) 1953.
[24] V. Hacker, G. Faleschini, H. Fuchs, R. Fankhauser, G. Simader, M. Ghaemi, B. Spreitz, K. Friedrich, J. Power Sources 71 (1998) 226.
[25] W. Malcolm, J. Chase (Eds.), NIST-JANAF Thermochemical Tables, fourth ed., American Institute of Physics, Woodbury, New York, 1998.
[26] G. van Rossum, S.R.A. Kersten, W.P.M. van Swaaij, Ind. Eng. Chem. Res. 46 (2007) 3959.
[27] M.J. Wornat, B.G. Porter, N.Y.C. Yang, Energy Fuels 8 (1994) 1131.
[28] X. Guo, Y. Sasaki, Y. Kashiwaya, K. Ishii, Mettal. Mater. Trans. B 35 (2004) 517.
[29] L. von Bogdandy, H.-J. Engell, The Reduction of Iron Ores: Scientific Basis and Technology, Springer-Verlag, Berlin, 1971.
[30] T. Wiltowski, K. Piotrowski, H. Lorethova, L. Stonawski, K. Mondal, S.B. Lalvani, Chem. Eng. Process. 44 (2005) 775.
[31] A.J. Fortini, D.D. Perlmutter, AIChE J. 35 (1989) 1245.
[32] K. Piotrowski, K. Mondal, H. Lorethova, L. Stonawski, T. Szymanski, T. Wiltowski, Int. J. Hydrogen Energy 30 (2005) 775.
[33] S. Takenaka, K. Otsuka, Energy Fuels 18 (2004) 820.
[34] S. Takenaka, T. Kaburagi, C. Yamada, K. Nomura, K. Otsuka, J. Catal. 228 (2004) 66.
[35] K. Otsuka, T. Kaburagi, C. Yamada, S. Takenaka, J. Power Sources 122 (2003) 111.
[36] M. Thaler, V. Hacker, M. Anilkumar, J. Albering, J.O. Besenhard, H. Schrottner, M. Schmied, Int. J. Hydrogen Energy 31 (2006) 2025.
[37] S.R.A. Kersten, Biomass Gasification in Circulating Fluidized Beds, University of Twente, Enschede, 2002.
[38] O. Levenspiel, D. Kunii, Fluidization Engineering, second ed., Butterworth-Heineman, Boston, 1991.